

Revisiting Effects of Nitrogen Incorporation and Graphitization on Conductivity of Ultra-nano-crystalline Diamond Films

Tanvi Nikhar,^{1,*} Robert Rechenberg,² Michael Becker,² and Sergey V. Baryshev^{1,†}

¹*Department of Electrical and Computer Engineering,
Michigan State University, 428 S. Shaw Ln., East Lansing, MI 48824, USA*

²*Fraunhofer USA Inc., Center for Coatings and Diamond Technologies
1449 Engineering Research Ct., B100 East Lansing, MI 48823, USA*

Detailed structural and electrical properties of ultra-nano-crystalline diamond (UNCD) films grown in $H_2/CH_4/N_2$ plasma were systematically studied as a function of deposition temperature (T_d) and nitrogen content (% N_2) to thoroughly evaluate their effects on conductivity. T_d was scanned from 1000 to 1300 K for N_2 fixed at 0, 5, 10 and 20 %. It was found that even the films grown in the synthetic gas mixture with no nitrogen could be made as conductive as $1-10^{-2} \Omega \text{ cm}$ with overall resistivity of all the films tuned over 4 orders of magnitude through varying growth parameters. On a set of 27 samples, Raman spectroscopy and scanning electron microscopy show a progressive and highly reproducible film material phase transformation, from ultra-nano-crystalline diamond to nano-crystalline graphite as deposition temperature increases. The rate of this transformation is heavily dependent on N_2 content. Addition of nitrogen greatly increases the amount of sp^2 bonded carbon in the films thus enhancing the physical connectivity in the GB network that have high electronic density of states. However, addition of nitrogen greatly slows down crystallization of sp^2 phase in the GBs. Therefore, proper balance between GB connectivity and crystallinity is the key in conductivity engineering of (N)UNCD.

I. INTRODUCTION

Diamond electronics faces great challenges due to the lack of low activation energy dopants. To allow room temperature operation, non-conventional concepts e.g. surface transfer doping [1–3] have been developed. p -type doping with boron [4] aided with surface transfer doping has helped achieve high performance devices with extremely low activation energy [5]. Still, to date, problems with n -type doping of diamond [6, 7] have hindered its development as a ubiquitous device material. Doping of bulk diamond with nitrogen (common donor impurity) produces a deep level 1.7 eV below the conduction band minimum. Other n -type dopants, such as sulfur and phosphorus, have been attempted with only limited success as the room-temperature conductivity was too low for applying these materials in conventional electronic device architectures. A shallow donor species is still sought for diamond.

Ultra-nano-crystalline diamond (UNCD) is another form of synthetic diamond which is shown to exhibit outstanding and tunable n -type conductivity, and excellent biocompatibility [8–11], thus enabling a range of applications toward high power and bio-medical devices. Typically, conductivity is tuned through adding N_2 or ammonia gas to the precursor gas mixture. Nitrogen modifies the morphology [12] and leads to orders of magnitude change in the electrical conductivity [13]. This physical picture is rooted in theoretical models that predict grain boundaries (GB) contained in UNCD induce specific sp^2

electronic defect states in the fundamental band gap of sp^3 diamond. When nitrogen is added, it preferentially incorporates into the GB and further increases density of defect states turning them into bands capable of transferring the charge. At the same time, a strong morphology change [12, 13] resulting in enhanced GB size increases connectivity in the touching GB forming conducting networks [14].

Despite significant progress in terms of applications, some fundamental aspects related to nitrogen incorporation into UNCD remained unaddressed. For example, the conductivity was found to saturate after attaining a certain nitrogen content in the plasma, which was further attributed to possible nitrogen incorporation saturation in UNCD [13, 15]. The specific nitrogen content in the precursor plasma required to obtain the maximum saturated conductivity value has large uncertainty [15, 16]. All the studies with varying nitrogen content were reported at a constant deposition temperature (T_d), and nitrogen was claimed to play the key role in setting high semi-metallic conductivity. Later, Ikeda *et al.* found strong dependence of conductivity on T_d . Addition of nitrogen played modest role [17]. Most recently, Alcantar-Pena *et al.* [18] achieved exceptional conductivity tunability, up to 100 S/cm, in undoped (0% N_2 in plasma) UNCD by simply varying T_d . Since both T_d (through fundamental diamond-to-graphite phase transition) and N_2 content (through volume inflation upon incorporation) can promote sp^2 phase formation, the relative strength of both processes and corresponding material transformations merit additional investigations. The studies conducted in Refs.[17, 18] were either restricted to limited number of T_d or N_2 values.

The present work is motivated from the described inconsistencies and lack of complete understanding of the

* nikharta@msu.edu

† serbar@msu.edu

factors responsible for conduction in (N)UNCD films. The objective of this work is therefore to systematically vary both N_2 content and T_d to revisit and better assess the physical origins transforming UNCD material from high to low resistivity state.

II. EXPERIMENT

UNCD films were grown on ultrasonically seeded intrinsic Si (100) substrates using microwave plasma chemical vapor deposition technique in a reactor operated at 2.45 GHz [19]. Four different series of samples were grown from a hydrogen rich $H_2/N_2/CH_4$ feed gas mixture with 0, 5, 10, and 20% of nitrogen (volume %), which corresponded to flow rates of 0, 10, 20 and 40 standard cubic centimeters per min (sccm) of N_2 . The CH_4 flow rate was kept constant at 10 sccm (5% by volume), while the flow rate of N_2 and H_2 was varied to maintain a total flow rate of 200 sccm. Different deposition temperatures were achieved ranging 1043 to 1295 K by varying the total pressure of the vacuum chamber (35 to 60 torr) and the input microwave power (2.5 to 3.0 kW). The substrate temperature was measured using an infrared pyrometer during a growth process of 60 minutes for each sample.

All samples were characterized using Horiba Raman spectrometer with 532 nm probing laser. High resolution scanning electron microscopy (SEM) was performed using a JEOL JSM 7500F to study the surface and bulk morphology. Four-point probe measurements were used to calculate the resistivity of the films using the thickness

calculated from (1) the weight measurements done before and after the growth process using a Mettler Toledo XS105 balance, and (2) reflectance interferogram measurements were performed using a Shimadzu UV-vis 2600 cross validated using SEM cross-section imaging. Surface roughness measurements were taken using Dektak 6M profilometer.

III. RESULTS AND DISCUSSION

The four different UNCD sample sets, totalling 27 samples, that were synthesized at four different nitrogen concentrations 0, 5, 10 and 20% are further labeled SA, SB, SC and SD, respectively. The following tables (Table I, II, III and IV for series SA, SB, SC and SD respectively) summarize the resultant properties of each series of films and the values of input parameters used to tune T_d . As seen, control of T_d was achieved by varying the input parameters *viz.* the forward microwave power and total pressure in the chamber. An increase in the substrate temperature was observed as nitrogen was increased in the plasma (replacing hydrogen) while all other input parameter values were kept fixed. Since the amount of nitrogen in the plasma dominated the substrate temperature, this effect could be explained in terms of how the energy is transferred from the gas molecules/ions to the substrate. N_2 is a heavier molecule compared to H_2 , and thus the energy transfer resulting from the bombardment of the substrate with N_2 is more efficient leading to higher T_d .

Sample	t_{weight} (nm)	t_{UV-vis} (nm)	Sheet Resistance R_s ($k\Omega/\square$)	Resistivity (Ωcm)	Avg. Roughness R_a (nm)	Peak to peak Roughness R_z (nm)	Deposition Temperature (Kelvin)	Deposition Time (hrs)	Total Pressure (sccm)	CH_4	N_2	Forward Power (W)
SA1	463	499.6	Too high		1.44	8.85	1048	1	40	5%	0%	2500
SA2	659	550.4	3.5×10^3	192.64	2.82	20.85	1098	1	45	5%	0%	3000
SA3	657	NA	30.8	2.025	1.66	9.22	1126	1	50	5%	0%	3000
SA4	532	NA	6.4	0.341	1.5	8.14	1156	1	55	5%	0%	3000
SA5	525	NA	0.297	0.015	2.11	10.61	1213	1	57	5%	0%	3000
SA6	687	NA	0.128	0.009	3.19	18.02	1248	1	60	5%	0%	3000

TABLE I: Series SA films grown with 0% N_2 concentration

Sample	t_{weight} (nm)	t_{UV-vis} (nm)	Sheet Resistance R_s ($k\Omega/\square$)	Resistivity (Ωcm)	Avg. Roughness R_a (nm)	Peak to peak Roughness R_z (nm)	Deposition Temperature (Kelvin)	Deposition Time (hrs)	Total Pressure (sccm)	CH_4	N_2	Forward Power (W)
SB1	456	393.52	15×10^3	590.2	4.2	19.34	1043	1	35	5%	5%	2500
SB2	541	528.9	5×10^3	264.4	4.47	24.61	1085	1	40	5%	5%	2500
SB3	498	518.4	12.56	0.65	4.83	18.78	1103	1	40	5%	5%	2700
SB4	636	584.37	20.63	1.2055	1.88	13.55	1118	1	45	5%	5%	2500
SB5	595	539.5	20.5	1.106	1.7	12.02	1125	1	45	5%	5%	2700
SB6	479	NA	3.76	0.1803	1.83	14.9	1148	1	43	5%	5%	3000
SB7	481	NA	5.29	0.2544	4.51	21.6	1151	1	45	5%	5%	3000
SB8	453	NA	2.74	0.124	2.09	9.93	1163	1	50	5%	5%	3000
SB9	532	NA	0.17	0.009	2.76	14.79	1229	1	60	5%	5%	3000

TABLE II: Series SB films grown with 5% N_2 concentration

Sample	t_{weight} (nm)	$t_{\text{UV-vis}}$ (nm)	Sheet Resistance R_s ($k\Omega/\square$)	Resistivity (Ωcm)	Avg. Roughness R_a (nm)	Peak to peak Roughness R_z (nm)	Deposition Temperature (Kelvin)	Deposition Time (hrs)	Total Pressure (sccm)	CH ₄	N ₂	Forward Power (W)
SC1	391	344.69	4×10^3	137.87	2.13	19.02	1068	1	35	5%	10%	2500
SC2	500	484.13	42.9	2.077	2.68	20.51	1101	1	40	5%	10%	2500
SC3	627	595.27	50.38	2.999	2.27	22.7	1145	1	45	5%	10%	2700
SC4	497	513.58	13.5	0.69	1.88	16.72	1163	1	45	5%	10%	3000
SC5	517	NA	0.66	0.034	2.39	12.17	1223	1	55	5%	10%	3000

TABLE III: Series SC films grown with 10% N₂ concentration

Sample	t_{weight} (nm)	$t_{\text{UV-vis}}$ (nm)	Sheet Resistance R_s ($k\Omega/\square$)	Resistivity (Ωcm)	Avg. Roughness R_a (nm)	Peak to peak Roughness R_z (nm)	Deposition Temperature (Kelvin)	Deposition Time (hrs)	Total Pressure (sccm)	CH ₄	N ₂	Forward Power (W)
SD1	194	223.16	30×10^3	669.48	2.44	21.51	1115	1	35	5%	20%	2500
SD2	279	239.66	12×10^3	287.6	2.13	18.61	1138	1	40	5%	20%	2500
SD3	371	325.31	2×10^3	65.06	2.81	21.01	1195	1	45	5%	20%	3000
SD4	367	398.96	19.7	0.786	3.53	27.86	1220	1	50	5%	20%	3000
SD5	552	NA	8.36	0.46	3.15	18.5	1259	1	55	5%	20%	3000
SD6	479	NA	4.7	0.225	2.79	18.9	1263	1	60	5%	20%	3000
SD7	365	NA	1.45	0.053	2.56	14.73	1295	1	65	5%	20%	3000

TABLE IV: Series SD films grown with 20% N₂ concentration

A. Resistivity

The room temperature resistivity of the films as a function of deposition temperature T_d measured with an optical pyrometer is shown in Fig. 1. A variation of ± 10 K (ΔT_{d1}) was observed based on different viewing angles along with a standard temperature variation of ± 5 K (ΔT_{d2}) during the one hour growth. A resultant error bar of ± 11.2 K for the x -axis is thus calculated taking both these variations into account, as $(\Delta T_{d1}^2 + \Delta T_{d2}^2)^{1/2}$.

Fig. 1 presents a direct comparison of resistivity variation for undoped and nitrogen incorporated UNCD films synthesized at different T_d . The resistivity decreases exponentially by more than four orders of magnitude from $\sim 10^2$ to 10^{-2} Ω cm as T_d changes by about 25%. The exponential decay hits the bottom at a resistivity that corresponds to a conductivity of ~ 100 S/cm. Room temperature (RT) conductivity of 100 S/cm is the champion conductivity value of (N)UNCD films claimed to be found only at N₂ concentration $>10\%$ in the precursor plasma [13, 20]. Important note is that the RT conductivity of (N)UNCD films has been shown insensitive to the ambient temperature [13, 14], which is a characteristic semi-metallic behaviour. In our case, the champion conductivity can be achieved for any nitrogen concentration, even 0%, through finding proper T_d . This result may look unusual but is supported by a few extensive experimental reports that widely varied the deposition temperature at constant N₂ concentrations, see for instance Refs.[17, 18]. Ikeda *et al.* [17] concluded that sp^2 phase in GB (dependent upon T_d) had to play significant role in setting conductivity. Pondering upon literature results [12, 16], it becomes clear that N₂ incorporation affects conductivity by increasing the sp^2 content in GB. It is important to note that while the trend and resistiv-

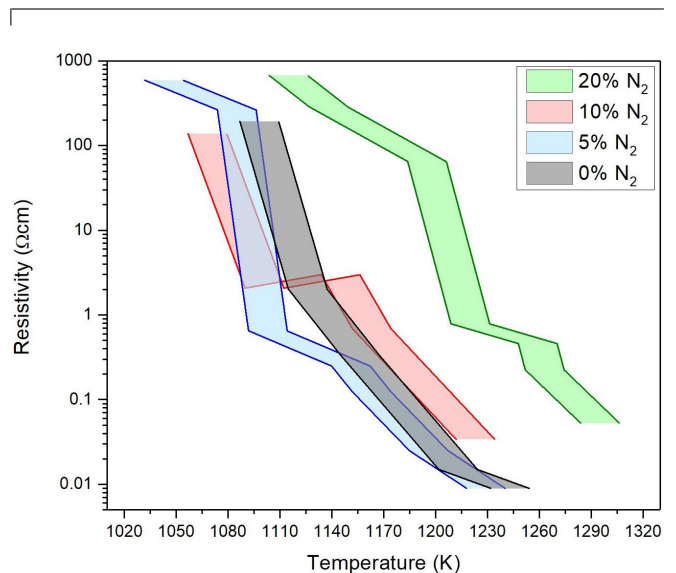


FIG. 1: Resistivity of all the films of series SA, SB, SC and SD as a function of deposition temperature

ity values recorded in Fig.1 are in accordance with the increasing T_d for a constant N₂ percentage, it is not the same for the increasing N₂ content for a constant T_d . It can be seen from Fig. 1 that for a given T_d , the higher the N₂ the higher the resistivity – this contradicts previous findings [13, 20].

Since it is the GBs that were found to be a common effect and source of inconsistencies including the newly found, it was hypothesized that the actual physical structure of GBs driven by thermo-chemical processes during plasma growth (rather than global plasma parameters such as T_d and N₂) must be related to the resistivity. Therefore, a closer look is taken at Raman spectroscopy

response of UNCD to evaluate diamond sp^3 and especially GB sp^2 transformations caused by the change of T_d and N_2 .

B. Raman Spectroscopy

Indeed, Raman spectroscopy is the most prominent method in determining structure of carbon-based electronic materials. The Raman of (N)UNCD features two major optical bands called D and G. Monitoring $I(D)/I(G)$ ratio was proposed for diamond-to-graphite ratio evaluation [refs1,2,3].

Other studies [refs1,2,3] provided large sets of Raman spectra that showed remarkable material transformations in that the intensities of the D and G bands non-monotonically changed as N_2 and T_d was varied. It revealed that the (N)UNCD material is highly "dynamic" upon being synthesized. Careful analysis of literature material [refs1,2,3] yields that not only intensities of the D and G bands change but so do their spectral line positions. For example, there is a clear and steady shift of the G band peak towards higher wavenumbers as T_d increases. To the best of our knowledge this effect has never been systematically studied and addressed.

The Raman spectra collected for all the four series SA, SB, SC and SD exhibit some prominent common features described as follows

1) A band with the peak position ranging between 1333 cm^{-1} and 1350 cm^{-1} . The 1333 cm^{-1} peak is the characteristic diamond peak attributed to sp^3 bonded carbon. The 1350 cm^{-1} feature appears for graphitic materials in the form of a band induced by the defect or disorder in the sp^2 bonded carbon. Polycrystalline graphite exhibits D band in its Raman spectrum due to the outer rim of graphite crystallites which tends to have more defects as opposed to the inside of the graphite crystal for which the band is not present [21]. In this discussion, this band will be referred to as the D band as has been used traditionally for systems containing mixed phases of sp^2 and sp^3 bonded carbon: D band contains two D's in its name, one is for sp^3 (D)iamond and another one is for sp^2 (D)efect. In further support of this statement, the films of the SD series allow for resolving two features in the D band as can be seen in Fig.3: one feature centers at 1333 cm^{-1} and is interpreted to be due to sp^3 bonded carbon and the second one centers at 1364 cm^{-1} and is due to disordered sp^2 bonded carbon.

2) A band with the peak position ranging between 1545 cm^{-1} and 1590 cm^{-1} which can be recognized as the G band. In addition to the D band, graphitic materials also exhibit a band at 1588 cm^{-1} called the G band attributed to the crystalline graphitic structure with sp^2 bonded carbon. The integrated intensity ratio of the D and G bands, $I(D)/I(G)$, is directly proportional to the defect quantity in graphitic sp^2 materials and inversely proportional to the in-plane crystallite size.

3) A shoulder at 1140 cm^{-1} and a weak peak at

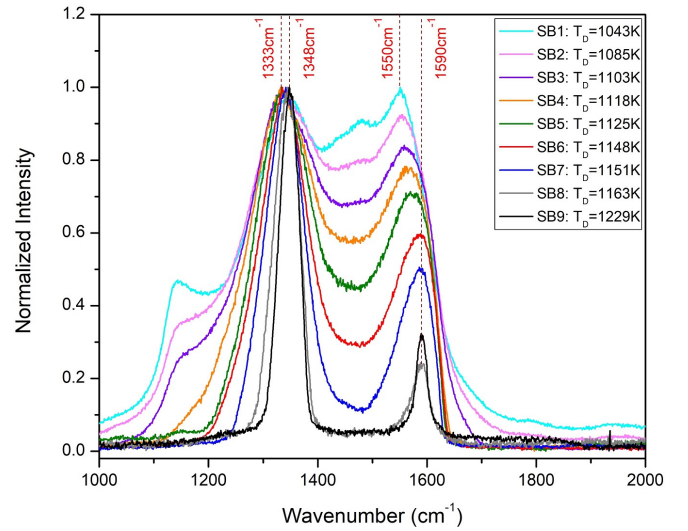


FIG. 2: Raman spectra for 5% N_2 samples as a function of T_d

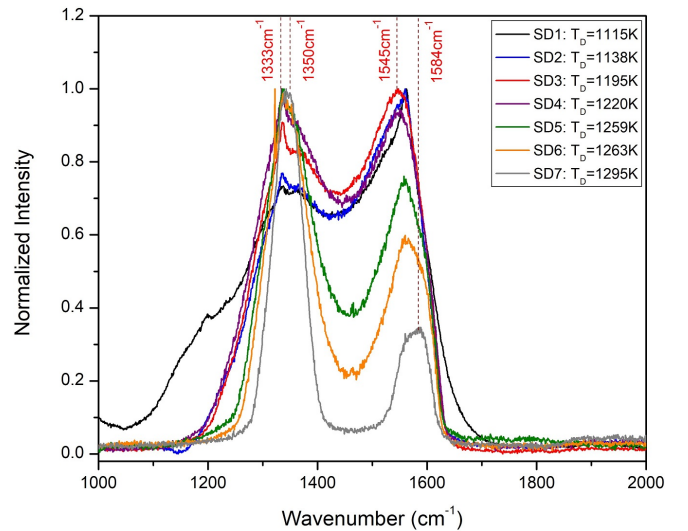


FIG. 3: Raman spectra for 20% N_2 samples as a function of T_d

1480 cm^{-1} representing ω_1 and ω_3 modes of trans-polyacetylene (t-PA) chains respectively.

The Raman spectra studied both as a function of T_d and N_2 percentage show various trends in the position, intensity and shape of the D, G, ω_1 and ω_3 peaks discussed as follows.

1. Raman spectra as a function of T_d

Fig. 2 shows the Raman spectra of films from SB series, grown with 5% N_2 in the feed gas mixture, for various T_d . As the temperature increases, the G band peak shifts from 1550 cm^{-1} to 1590 cm^{-1} with decreasing intensity which shows a reduction of the amorphous

carbon content and its conversion from short-range to long range order [22]. The peak shift is also accompanied by its narrowing indicating an increase in the crystallinity of the material. Thus, with the increase in T_d , the sp^2 bonded carbon changes from amorphous to polycrystalline graphite. The high intensity of defect-induced D band with respect to G band can be attributed to a large volume of edges resulting from small size GBs lining the diamond grains.

For lower T_d , the D band is broad with its peak weighted at 1333 cm^{-1} . As T_d increases to up to 1148 K, the band gets narrower while its peak spectral position stays constant at 1333 cm^{-1} . Beyond 1148 K, the D band continues to get narrower and the peak at 1333 cm^{-1} instantaneously moves to 1350 cm^{-1} , indicating that there is no sp^3 carbon to be detected by Raman spectroscopy. The most striking transformation takes place within the SD series (Fig. 3). The 1333 cm^{-1} diamond peak keeps intensifying with respect to the 1350 cm^{-1} peak as T_d increases upto 1195 K which shows the most optimal condition to synthesize (N)UNCD films of the largest fraction of diamond content. For $T_d > 1195$ K, the peaks merge together and shift completely to 1350 cm^{-1} at 1295 K. This complete D band peak shift from 1333 cm^{-1} to 1350 cm^{-1} taking place at higher synthesis temperatures suggests the UNCD material converts from diamond sp^3 host matrix containing graphitic GBs to crystallized nano-graphite – this is normal to expect due to the existence of fundamental phase transition at ~ 1500 K from metastable diamond structure to its fundamental ground state which is graphite. The fact that this phase transformation happens at lower temperature is due to ultra-small (~ 10 nm) diamond grains enhancing the kinetic rate. The phenomenon of UNCD converting into other carbon structures when exposed to high temperatures, is also in agreement with previous results [18, 23].

The spectral features at 1140 cm^{-1} and 1480 cm^{-1} de-intensify as T_d increases and completely disappear after 1103 K: these are ω_1 (in-plane C-H bending combined with C-C stretching) and the ω_3 (C=C stretching) vibration modes of t-PA chains. Accordingly, these features were associated with fragments of t-PA-like species also present in the grain boundaries. The disappearance of these features due to t-PA decomposition also confirms that these modes of t-PA are not related to diamond grains [24]. The removal of t-PA chains present in the grain boundaries also aids to the formation of better sp^2 bonded phase in GBs.

Quenching of t-PA spectral features was observed for all other sets, SA, SC and SD, to happen at near 1100 K, and was a convenient benchmark reference for temperature reliability measurement. Likewise, as seen in Fig. 4, 5 and 3, the trends of the D and G bands of Raman spectra of other three sets were consistent with the results outlined in regards to Fig. 2. For increasing T_d irrespective of the concentrations of nitrogen in the plasma, the common trends, yielding consistency behind

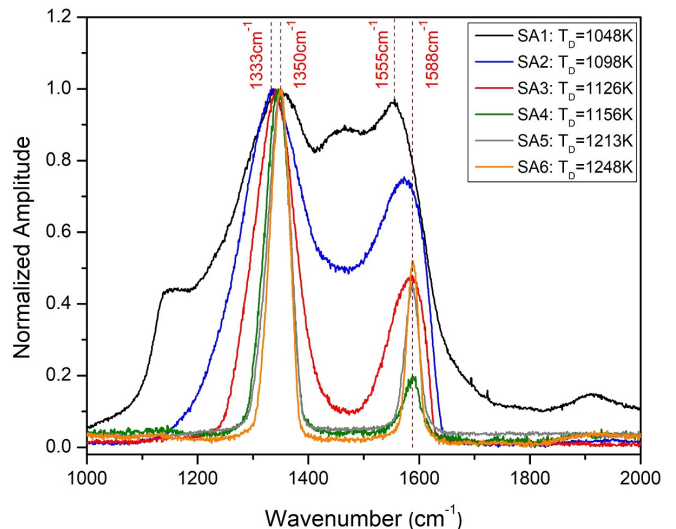


FIG. 4: Raman spectra for 0% N_2 samples as a function of T_d

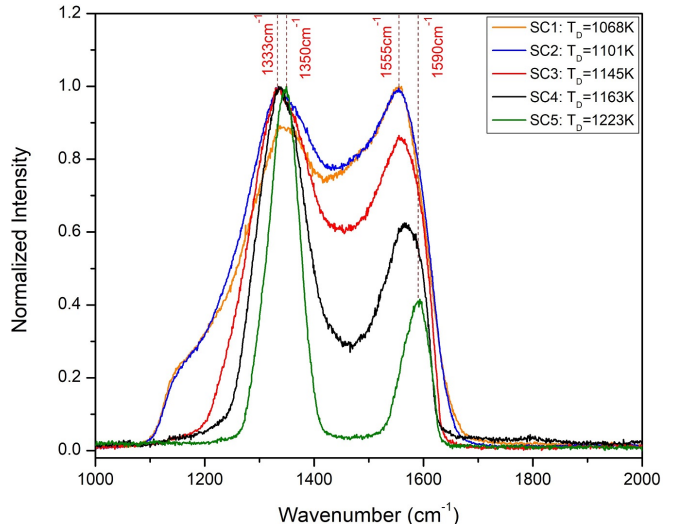


FIG. 5: Raman spectra for 10% N_2 samples as a function of T_d

the argument on material transformation from UNCD to nano-crystalline graphite, can be summarized as follows

- 1) The shift in the D band peak from 1333 cm^{-1} to 1350 cm^{-1} along with the narrowing of the band.
- 2) The decrease in the intensity and the shift in the G band peak from 1550 cm^{-1} to 1590 cm^{-1} along with the narrowing of the band.
- 3) The decrease and quench of the t-PA features at 1140 cm^{-1} and 1480 cm^{-1} . These features disappear after about 1100 K for all the four series of films which again confirms that these are not related to diamond.

2. Raman spectra as a function of N_2 in the feed gas

Figures 6 and 7 demonstrate comparison sets of Raman spectra for (N)UNCD films that were grown at the same T_d of 1098 K and 1126 K respectively, but with varied N_2 content. For T_d kept constant, the comparison of the peak intensity of the G band shows that the amount of sp^2 phase increases with increasing N_2 concentration in the growth plasma. Combined with the result in Fig. 3, it does show that both sp^2 GB size and sp^3 diamond grain size are inflated by adding more nitrogen [12]. There is an important *nuance* that exists: as the G peak increases with N_2 content, its position moves toward smaller wavenumbers. It means that even though the relative size of GB (i.e. the available conduction channel) is increased, such GBs are not of good use as they are largely amorphous. Therefore, it is concluded that N_2 alone is not a prerequisite for engineering high conductivity in 10% and 20% films. This is consistent with the major result presented in Fig. 1.

GB amorphization induced by the increasing nitrogen content can be thought of as result of the changing amount of energy required in the formation of increasing amount of CN bonds. The positive enthalpy of formation of many CN bonds [25] could make the incorporation of nitrogen in the GBs of UNCD an endothermic process. Thus, the available thermal energy in the CVD reactor needs to be increased via increasing T_d to enable (1) the incorporation of nitrogen through the formation of CN bonds in the GB of the films, and (2) sp^2 GB crystallization. In other words, increasing CN bond formation for the incorporation of nitrogen leads to an overall increase in the required thermal energy to achieve the same level of crystallinity of sp^2 bonded carbon which is the major contributing factor towards the conductivity of the films. This hypothesis could account for (1) the increased amount of amorphous sp^2 phase in high N_2 % films and (2) the upward shift in T_d required to obtain (N)UNCD films with similar resistivities for increasing nitrogen content in the plasma. For instance, the resistivity value of $\sim 0.6 \Omega\cdot\text{cm}$ was achieved at 1103 K with 5% N_2 as opposed to 1163 K for 10% N_2 and 1221 K for 20% N_2 .

C. Scanning electron microscopy

Extensive data set of electron micrographs of the surface of the films further corroborates the main conclusions and observations that came from Raman spectroscopy and add more insight into details of (N)UNCD growth. Figures 8, 9, 10 and 11 illustrate systematic and reproducible surface morphology of films that modifies with increasing T_d for 0, 5, 10 and 20% N_2 respectively.

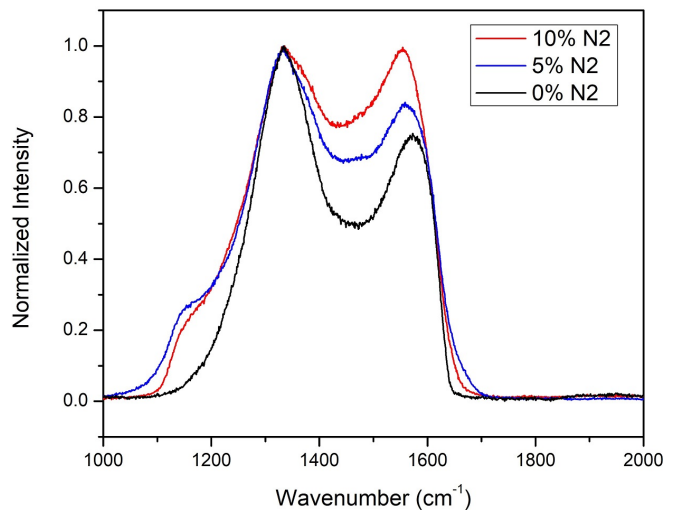


FIG. 6: Raman spectra for samples deposited at 1098 K with 0, 5 and 10% N_2 concentration

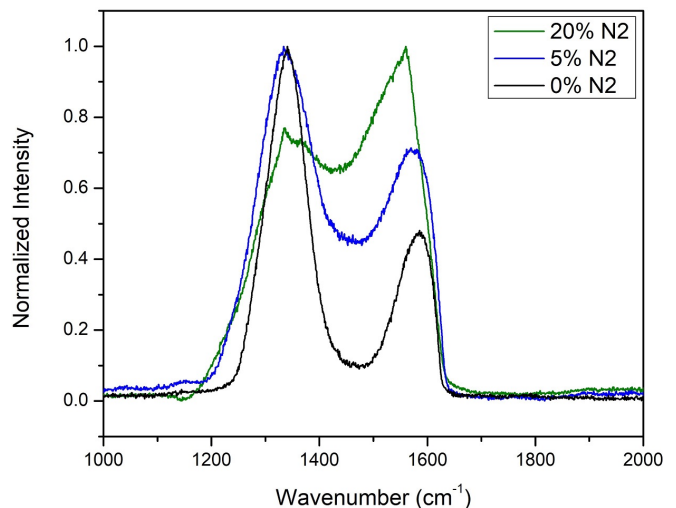


FIG. 7: Raman spectra for samples deposited at 1126 K with 0, 5 and 20% N_2 concentration

1. Changes in surface morphology with varying T_d

Comparison of the morphology of films grown at a particular nitrogen concentration shows a transition from UNCD to nanocrystalline graphite with increasing T_d . Films grown at lower T_d as shown in Fig. 8(a), 9(a), 10(a) and 11(a) exhibit densely packed nanometer sized diamond grains forming a continuous film and thus, confirming the growth of UNCD films. At higher deposition temperatures, it is seen that the amount of deposited graphite increases. Fig. 8(b), 9(b), 10(b) and 11(b) show the appearance of small voids that grow as T_d increases. These voids finally take form of ordered nano-platelets as seen in Fig. 8(c), 9(c), 10(c) and 11(c). This is in accordance with the transition in morphology from densely packed nano-diamond film to platelet packed semi-void

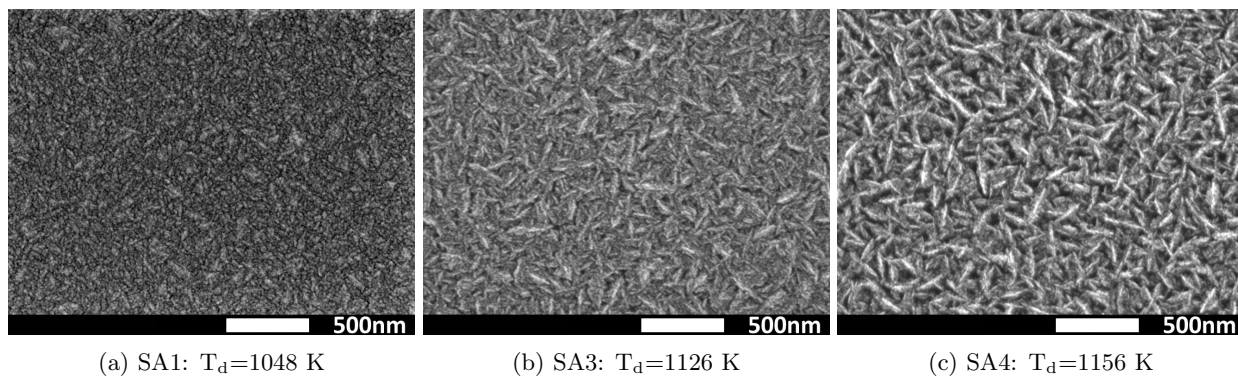


FIG. 8: SEM images of samples grown with 0% N_2 concentration

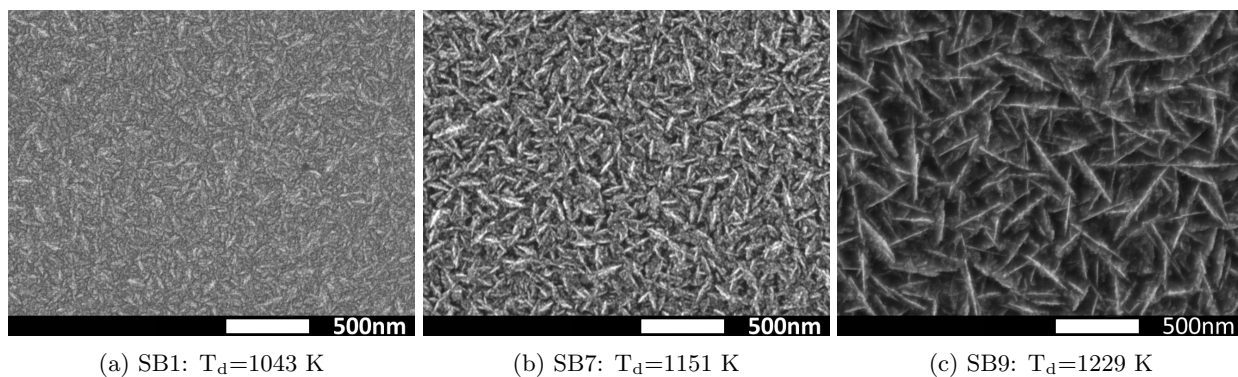


FIG. 9: SEM images of samples grown with 5% N_2 concentration

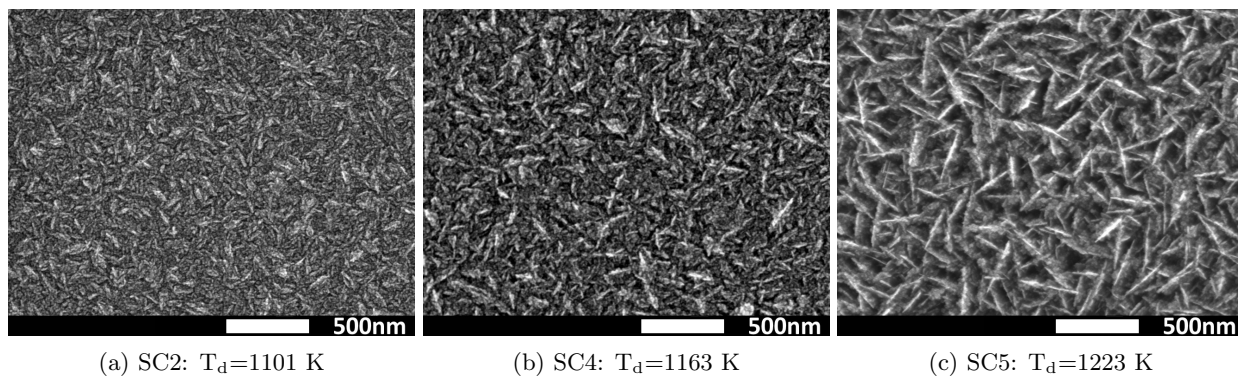


FIG. 10: SEM images of samples grown with 10% N_2 concentration

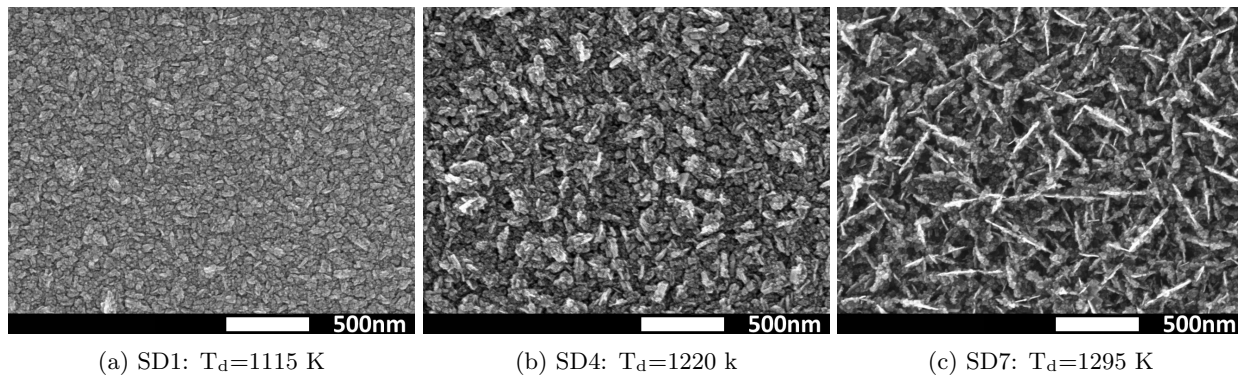


FIG. 11: SEM images of samples grown with 20% N_2 concentration

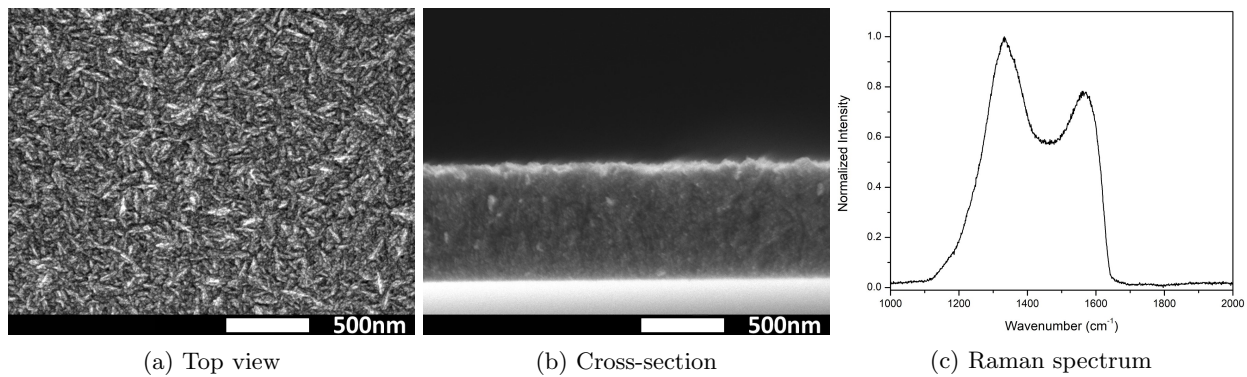


FIG. 12: SEM and Raman spectrum of sample: SB4, grown with 5% N_2

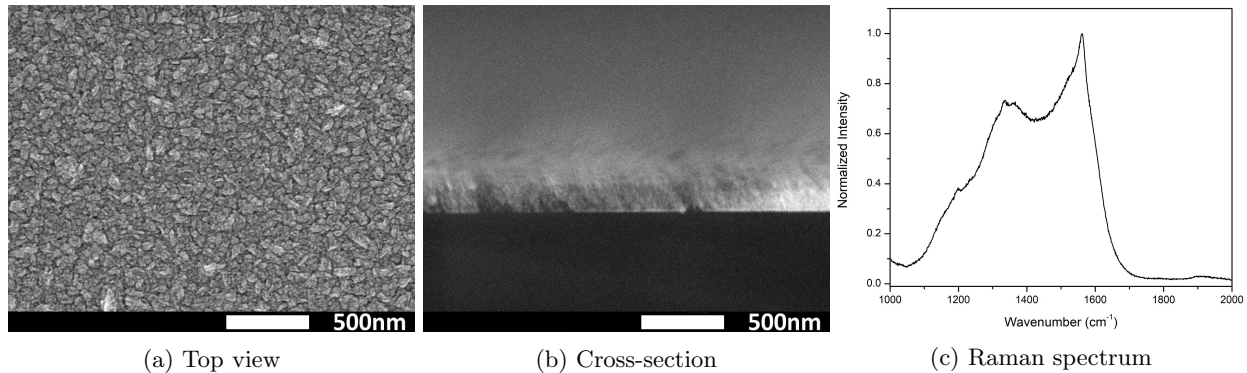


FIG. 13: SEM and Raman spectrum of sample: SD1, grown with 20% N_2

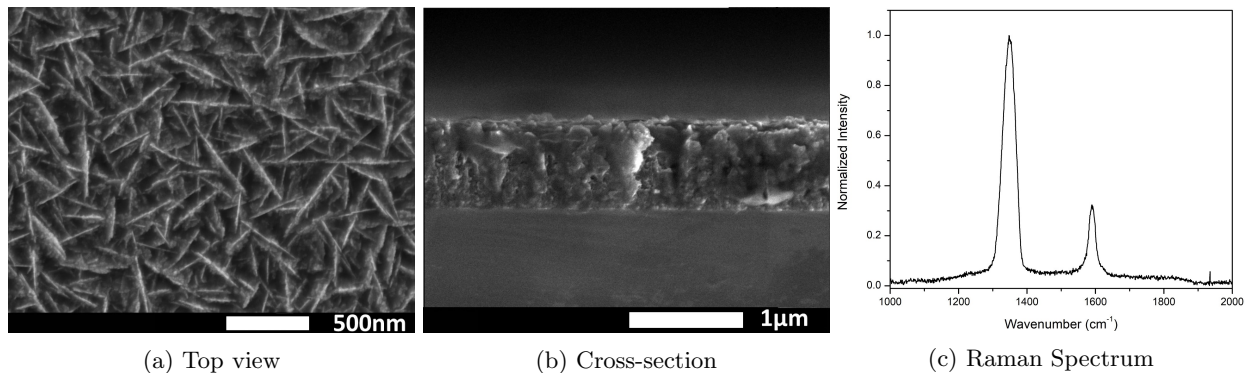


FIG. 14: SEM and Raman spectrum of sample: SB9, grown at high T_d

nano-graphite with increasing T_d reported earlier [23]. Therefore, the surface morphology results are consistent with the Raman results.

2. Changes in surface morphology with increasing N_2 concentration

Films grown at lower T_d reveal a sizable change in the grain size as nitrogen concentration is varied. For low N_2 concentration (Fig. 8(a), 9(a) for 0%, 5% N_2 respectively), films are small grained. Fig. 10(a) shows a slight increase in the grain size for 10% N_2 film. However, grain size increases significantly and the (N)UNCD of SD series

structure become coarse representing the strong influence of high nitrogen content (20% here) on sp^3 phase growth, as seen from Fig. 11(a). These results are in accordance with previously reported changes in grain size with varying nitrogen concentration [12, 13]. For the case of SD series, increase in T_d additionally makes the grain size larger such that diamond lattice faceting becomes visible. This is consistent with the Raman results presented in Fig. 3 that illustrated the diamond D band (1333 cm^{-1}) resolved from the defect D band (1350 cm^{-1}).

3. Cross section analysis

To obtain more insight into the difference between closely grain packed and platelet packed films, cross-sectional analysis was employed, see Figs. 12, 13 and 14. It is seen that the films grown at lower T_d show no identifiable columnar structure for both low and high nitrogen concentration samples – this is a canonical UNCD pattern due to high re-nucleation rate [26]. More specifically, the cross-section of 5% N_2 film in Fig. 12(b) shows smooth fracture cross-section of a highly dense continuous film with no columnar growth. The cross-section of 20% N_2 film in Fig. 13(b) also shows a highly dense film resulting from high renucleation rate along with discernable grains due to larger crystallite size as seen in Fig. 13(a).

Contrastingly, Fig. 14(b) shows the cross-sectional view of highly graphitized film (as interpreted from Raman) grown at a high T_d of 1229 K: the platelet observed in the top-view imaging thread through the entire film, from the substrate to the surface.

D. Graphitization

The significant change in the peak positions and width of the D and G bands has been noted for all the four series of films. It was interpreted to be due to material transition from nano-sized diamond grains surrounded by amorphous sp^2 carbon liner to nanocrystalline graphite. This interpretation was further supported by top-view and cross-sectional SEM imaging. To even further corroborate this argument and confirm the process of graphitization in the films, a comparison with single crystal diamond (SCD), a pure sp^3 case, and highly oriented pyrolytic graphite (HOPG), a pure sp^2 case, was drawn. Raman spectra (Fig. 15) of SCD with peak at 1333 cm^{-1} and HOPG with peak at 1582 cm^{-1} are compared to a 0% N_2 UNCD grown at three highest temperatures, 1156, 1213 and 1248 K. As was evident from Fig. 4, the intensity of G band peak at 1550 cm^{-1} of the 0% N_2 films keeps decreasing owing to the decrease in the amorphous content in the film along with the shift of the peak position from 1550 cm^{-1} to 1588 cm^{-1} . When the peak has completely shifted to 1588 cm^{-1} , it does not change its position any further with an increase in T_d beyond 1156 K and starts re-intensifying again as shown now in Fig. 15. The increase in the 1588 cm^{-1} peak shows an increase in the amount of crystalline sp^2 phase. The absence of the diamond peak feature within the D band and the presence of the G band in the spectra of 0% N_2 films (as opposed to single G band spectrum of HOPG) confirms that now the material grows completely as nanocrystalline graphite. The increase in the crystallinity of sp^2 phase is also evident from Fig. 2 for the 5% N_2 films where G band peak completely shifts to 1590 cm^{-1} at 1163 K and starts intensifying for higher T_d .

A similar material transition was also observed in our

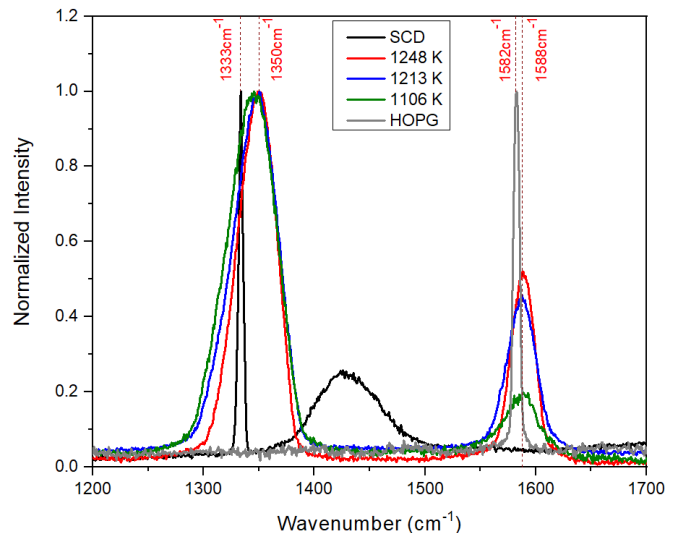


FIG. 15: Comparison of Raman spectra of highly graphitized films with single crystal diamond and highly oriented pyrolytic graphite

study of glow discharge plasma during field emission from UNCD cathodes [27] where data from SEM and Raman showed the conversion of nano-diamond to nano-graphite caused by the electron emission self-induced heating of the emitter to 2000–4000 K.

The most direct confirmation of graphitization comes from mass density evaluation. We compare the actual thickness measurement from the cross-section SEM imaging (t_{SEM}) with indirect thickness estimation from the weight difference before and after growth (t_{weight}) using the density of pure diamond ($\rho_{dia}=3.51\text{ g/cm}^3$) and graphite ($\rho_{gra}=2.27\text{ g/cm}^3$). As seen from Table. V, t_{SEM} values are in close match with t_{weight} calculated using ρ_{dia} for samples grown at low T_d (Samples 1 and 2), thus confirming they largely retain the structural property of diamond (Raman spectra of these samples are presented in Fig. 16). For high T_d though, t_{weight} only matches t_{SEM} if ρ_{gra} is used for calculation. Thus, Samples 3 and 4 (Raman spectra are in Fig. 16) largely retain the structural property of graphite.

Sample	t_{SEM} (nm)	t_{weight} (nm) using ρ_{dia}	t_{weight} (nm) using ρ_{gra}
Sample 1	156	194	300
Sample 2	764	636	983
Sample 3	742	517	799
Sample 4	830	532	822

TABLE V: Comparison of thickness values obtained from SEM and weight density measurements

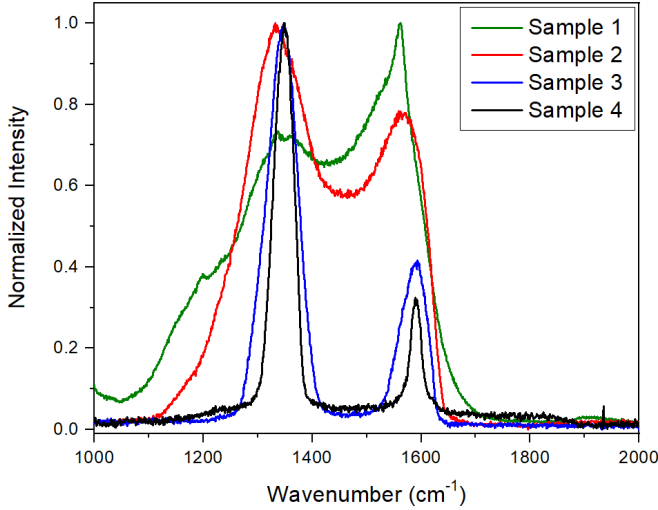


FIG. 16: Corresponding Raman spectra of the samples used for thickness comparison in Table V

A comparison of the reflectance spectrum obtained from UV-vis spectroscopy is shown in Fig. 17. High reflectance and strong interference pattern was exhibited by the bright pink sample SB1 deposited at 1043 K while low reflectance and no interference was observed for the highly graphitized sample SB9 grown at 1229 K. Both, mass density and optical analysis provide unambiguous proof of the fundamental material transition from UNCD to nanocrystalline graphite.

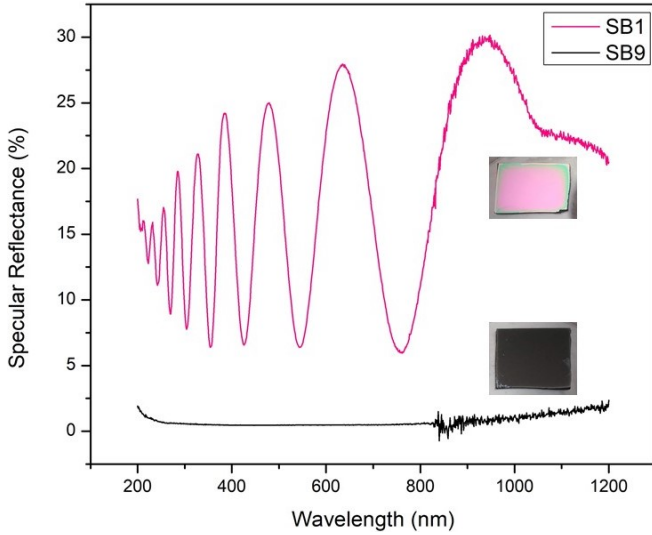


FIG. 17: Comparison of reflectance spectra of UNCD and highly graphitized film

E. Revisiting resistivity effects and attempting to redefine UNCD

Having confirmed the UNCD–nanographite transformation, a more universal chart behind resistivity effect,

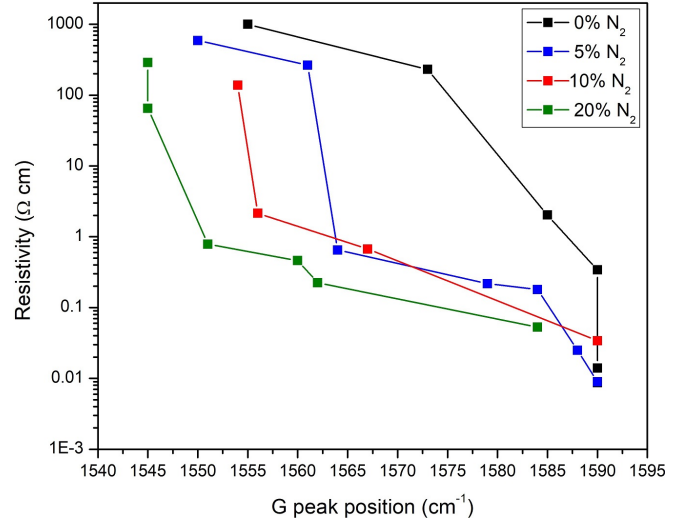


FIG. 18: Resistivity as a function of G peak position

that depends not only on N₂ content but also on T_d , can be drawn. It is proposed to plot resistivity as a function of G band position, as examples in Fig. 18, with G band position bound between 1550 cm⁻¹ to 1590 cm⁻¹. Four samples series are plotted. A few main features can be highlighted as follows:

- 1) The resistivity of series SD (20% N₂) has immediate and strong response to the G peak position: slight improvement in GB crystallinity (G band shifts by +5 cm⁻¹) drops resistivity by over 2 orders of magnitude;
- 2) Unlike series SD, series SA (0% N₂) is largely insensitive to the G band position (GB crystallinity) until after 1575 cm⁻¹.
- 3) As T_d reaches the highest values when all the films (regardless of N₂ content) turn into crystalline nanographite (G band is centered at 1590 cm⁻¹), it is not surprising to see that all the four film series converge to the same resistivity of $\sim 10^{-2}$ Ω·cm at the same G peak position centered at 1590 cm⁻¹.

As was demonstrated in Figs. 6 and 7, the increase of plasma nitrogen content simultaneously increases grain size and GB size. This is consistent with previous transmission electron microscopy results [12, 13] that found changing N₂ from 0% to 20% inflated the GB width from 0.5 to 2.2 nm and diamond grain size from 4 to 16 nm. If so, the following physical mechanism is proposed to interpret the result of Fig. 18. Higher N₂ content creates larger grain boundaries: it means larger density of state (DOS) in the π and π^* bands that reside inside the fundamental band gap of diamond [28–30], plus it increases the physical connectivity between touching GBs (contact area). Thus, at high N₂ concentration the large amount of charge is readily available and the cross section area of wired/interconnected GBs is large. Even so, at the lowest T_d , attempted in this work, the resistivity remains very high – this is because the charge carrier mean free path is small and so is the mobility due to amorphous struc-

ture in GBs. The role of increasing T_d is two-fold: (1) it keeps increasing the number of states in the π and π^* bands and (2) improves GB crystallinity yielding larger mean free path i.e. higher mobility. Contrastingly, 0% films have low connectivity and low DOS in the π and π^* bands at low T_d , and can only develop those metrics (plus improved mobility owing to improved crystallinity) if the synthesis temperature is increased. This is why the SD series is more prone to the G band peak position, having immediate response to the quality of sp^2 GBs, than the other series.

Tracing now the D band position in our Raman spectra data sets, one more universal conclusion could be made. The film could be referred to as UNCD as long as it has some diamond grain material in it. As was illustrated, presence of diamond material is signified by the presence of the D band centered at 1333 cm^{-1} peak, or at least an asymmetric left-hand shoulder of the D band extending toward 1333 cm^{-1} . The material fully transforms to nanocrystalline graphite when the D band completely shifts to nearby wavenumber 1350 cm^{-1} (at this point the D band is symmetric) and therefore no longer probes/detects diamond sp^3 content in the film but rather represents nanographite defect condition.

IV. CONCLUSION

Effects of nitrogen incorporation (via changing the N_2 content in the synthetic plasma from 0 to 20 %) and the deposition temperature T_d (via changing the total plasma pressure and input rf power from 1000 to 1300 K) on (N)UNCD resistivity were systematically investigated using a set of 27 samples.

Based on Raman spectroscopy (additionally supported by physical structure studies by SEM, spectrophotometry and weighing), charge transport can be explained based on two competitive processes. Addition of N_2 increases the sp^2 -bonded carbon comprising GBs, which yields enhanced spatial connectivity of grain boundaries and enhanced overlap between π and π^* states in the en-

ergy space. Together, these could make charge transport more facile causing resistivity to drop. In reality, resistivity does not drop until an elevated T_d improves crystallinity (enhancing mobility) of GBs because incorporated nitrogen amorphizes them. Larger the N_2 content, larger the T_d required to recover to the same resistivity. Therefore, there is a thermophysicochemical process that governs the structure and kinetics of the GB formation that is dependent on flow rates, total pressure and input rf power – this process is a function of the reactor design with T_d being a byproduct of the reactor settings/design. It is proposed to represent resistivity as function of the Raman G band peak position, one of the two main characteristic bands in UNCD (as well as other polycrystalline diamond and graphite materials) storing information about sp^2 grain boundary structure. This representation is not contingent on the reactor design and allows for relating the resistivity and structural quality of the final material product.

Practically speaking, this approach outlines a path of engineering resistivity of UNCD between $10^3 - 10^{-2}\ \Omega\text{ cm}$ even when containing no nitrogen. The downside of synthesizing UNCD at 0 % N_2 is that achieving resistivity of $10^{-1} - 10^{-2}\ \Omega\text{ cm}$ appealing for many applications requires T_d in excess of 1150 K (in our reactor design): at this point the material retains little or no signature of UNCD and is being transformed into nanographite. In contrast, enhanced connectivity between GBs in N_2 rich samples allows for achieving $10^{-1} - 10^{-2}\ \Omega\text{ cm}$ while maintaining high diamond fraction in UNCD, thanks to the slowed kinetics of the nanodiamond-to-nanographite phase transition taking place at T_d over 1250 K (in our reactor design).

ACKNOWLEDGMENTS

The authors would like to thank James E. Butler, Tim Hogan and Tim Grotjohn for useful discussions. TN and SVB were funded by the College of Engineering, Michigan State University, under the Global Impact Initiative.

-
- [1] M. I. Landstrass and K. V. Ravi, Resistivity of chemical vapor deposited diamond films, *Applied Physics Letters* **55**, 975 (1989).
 - [2] J. F. Prins, n-type semiconducting diamond by means of oxygen-ion implantation, *Phys. Rev. B* **61**, 7191 (2000).
 - [3] I. Sakaguchi, M. N.-Gamo, Y. Kikuchi, E. Yasu, H. Haneda, T. Suzuki, and T. Ando, Sulfur: A donor dopant for n-type diamond semiconductors, *Phys. Rev. B* **60**, R2139 (1999).
 - [4] S. A. Grot, C. W. Hatfield, G. S. Gildenblat, A. R. Badzian, and T. Badzian, Electrical properties of selectively grown homoepitaxial diamond films, *Applied Physics Letters* **58**, 1542 (1991).
 - [5] O. A. Williams, M. D. Whitfield, R. B. Jackman, J. S. Ford, J. E. Butler, and C. E. Nebel, Formation of shallow acceptor states in the surface region of thin film diamond, *Applied Physics Letters* **78**, 3460 (2001).
 - [6] S. Koizumi, T. Teraji, and H. Kanda, Phosphorus-doped chemical vapor deposition of diamond, *Diamond and Related Materials* **9**, 935 (2000).
 - [7] H. Kato, S. Yamasaki, and H. Okushi, n-type doping of (001)-oriented single-crystalline diamond by phosphorus, *Applied Physics Letters* **86**, 222111 (2005).
 - [8] O. Auciello, P. Gurman, M. B. Guglielmotti, D. G. Olmedo, A. Berra, and M. J. Saravia, Biocompatible ultrananocrystalline diamond coatings for implantable medical devices, *MRS Bulletin* **39**, 621629 (2014).
 - [9] O. Auciello and A. Sumant, Status review of the science

- and technology of ultrananocrystalline diamond (uncd (tm)) films and application to multifunctional devices, *Diamond and Related Materials* **19**, 699 (2010).
- [10] P. Bajaj, D. Akin, A. Gupta, D. Sherman, B. Shi, O. Auciello, and R. Bashir, Ultrananocrystalline diamond film as an optimal cell interface for biomedical applications, *Biomedical Microdevices* **9**, 787 (2007).
- [11] X. M. Xiao, J. Wang, C. Liu, J. A. Carlisle, B. V. Mech, R. G. Greenberg, D. S. Guven, R. Freda, M. S. Humayun, J. D. Weiland, and O. H. Auciello, In vitro and in vivo evaluation of ultrananocrystalline diamond for coating of implantable retinal microchips., *Journal of biomedical materials research B* **77** **2**, 273 (2006).
- [12] J. Birrell, J. A. Carlisle, O. Auciello, D. M. Gruen, and J. M. Gibson, Morphology and electronic structure in nitrogen-doped ultrananocrystalline diamond, *Applied Physics Letters* **81**, 2235 (2002).
- [13] S. Bhattacharyya, O. Auciello, J. Birrell, J. A. Carlisle, L. A. Curtiss, A. N. Goyette, D. M. Gruen, A. R. Krauss, J. Schlueter, A. Sumant, and P. Zapol, Synthesis and characterization of highly-conducting nitrogen-doped ultrananocrystalline diamond films, *Applied Physics Letters* **79**, 1441 (2001).
- [14] I. S. Beloborodov, P. Zapol, D. M. Gruen, and L. A. Curtiss, Transport properties of n-type ultrananocrystalline diamond films, *Phys. Rev. B* **74**, 235434 (2006).
- [15] P. Achatz, O. A. Williams, P. Bruno, D. M. Gruen, J. A. Garrido, and M. Stutzmann, Effect of nitrogen on the electronic properties of ultrananocrystalline diamond thin films grown on quartz and diamond substrates, *Physical Review B* **74** (2006).
- [16] J. Birrell, J. E. Gerbi, O. Auciello, J. M. Gibson, D. M. Gruen, and J. A. Carlisle, Bonding structure in nitrogen doped ultrananocrystalline diamond, *Journal of Applied Physics* **93**, 5606 (2003).
- [17] T. Ikeda, K. Teii, C. Casiraghi, J. Robertson, and A. C. Ferrari, Effect of the sp^2 carbon phase on n-type conduction in nanodiamond films, *Journal of Applied Physics* **104** (2008).
- [18] J. Alcantar-Pea, J. Montes, M. Arellano-Jimenez, J. O. Aguilar, D. Berman-Mendoza, R. Garca, M. Yacaman, and O. Auciello, Low temperature hot filament chemical vapor deposition of ultrananocrystalline diamond films with tunable sheet resistance for electronic power devices, *Diamond and Related Materials* **69**, 207 (2016).
- [19] J. Asmussen and D. K. Reinhard, *Diamond Films Handbook* (2010).
- [20] O. A. Williams, S. Curat, J. E. Gerbi, D. M. Gruen, and R. B. Jackman, n-type conductivity in ultrananocrystalline diamond films, *Applied Physics Letters* **85**, 1680 (2004).
- [21] M. A. Pimenta, G. Dresselhaus, M. S. Dresselhaus, L. G. Cançado, A. Jorio, and R. Saito, Studying disorder in graphite-based systems by Raman spectroscopy, *Physical Chemistry Chemical Physics* **9**, 1276 (2007).
- [22] A. C. Ferrari and J. Robertson, Interpretation of raman spectra of disordered and amorphous carbon, *Phys. Rev. B* **61**, 14095 (2000).
- [23] O. Grning, O. M. Kttel, P. Grning, and L. Schlapbach, Field emission properties of nanocrystalline chemically vapor deposited-diamond films, *Journal of Vacuum Science & Technology B* **17**, 1970 (1999).
- [24] R. Pfeiffer, H. Kuzmany, N. Salk, and B. Gnther, Evidence for trans-polyacetylene in nanocrystalline diamond films from hd isotropic substitution experiments, *Applied Physics Letters* **82**, 4149 (2003).
- [25] Q. Z. H. Dong, A. R. Oganov and G. R. Qian, The phase diagram and hardness of carbon nitrides, *Scientific Reports* **5** (2015).
- [26] D. M. Gruen, Nanocrystalline diamond films, *Annual Review of Materials Science* **29**, 211 (1999).
- [27] S. S. Baturin, T. Nikhar, and S. V. Baryshev, Field electron emission induced glow discharge in a nanodiamond vacuum diode, *Journal of Physics D* **52**, 325301 (2019).
- [28] M. Nešládek, K. Meykens, L. M. Stals, M. Vaněček, and J. Rosa, Origin of characteristic subgap optical absorption in cvd diamond films, *Phys. Rev. B* **54**, 5552 (1996).
- [29] P. Zapol, M. Sternberg, L. A. Curtiss, T. Frauenheim, and D. M. Gruen, Tight-binding molecular-dynamics simulation of impurities in ultrananocrystalline diamond grain boundaries, *Phys. Rev. B* **65**, 045403 (2001).
- [30] O. Chubenko, S. S. Baturin, and S. V. Baryshev, Theoretical evaluation of electronic density-of-states and transport effects on field emission from n-type ultrananocrystalline diamond films, *Journal of Applied Physics* **125**, 205303 (2019).